Lrp4 expression by adipocytes and osteoblasts differentially impacts sclerostin's endocrine effects on body composition and glucose metabolism

Received for publication, November 17, 2018, and in revised form, February 23, 2019 Published, Papers in Press, March 6, 2019, DOI 10.1074/jbc.RA118.006769

Soohyun P. Kim[‡], Hao Da[‡], Zhu Li[‡], Priyanka Kushwaha[‡], Conor Beil[‡], Lin Mei[§], Wen-Cheng Xiong[§], Michael J. Wolfgang[¶], Thomas L. Clemens[‡‖1], and Ryan C. Riddle[‡‖2]

From the Departments of [‡]Orthopedic Surgery and [¶]Biological Chemistry, Johns Hopkins University School of Medicine, Baltimore, Maryland 21205, the [§]Department of Neuroscience, Case Western Reserve University Medical School, Cleveland, Ohio 44106, and the [‖]Baltimore Veterans Affairs Medical Center, Baltimore, Maryland 21201

Edited by Qi-Qun Tang

Sclerostin exerts profound local control over bone acquisition and also mediates endocrine communication between fat and bone. In bone, sclerostin's anti-osteoanabolic activity is enhanced by low-density lipoprotein receptor–related protein 4 (Lrp4), which facilitates its interaction with the Lrp5 and Lrp6 Wnt co-receptors. To determine whether Lrp4 similarly affects sclerostin's endocrine function, we examined body composition as well as glucose and fatty acid metabolism in mice rendered deficient of Lrp4 in the adipocyte (AdΔLrp4) or the osteoblast (ObΔLrp4). AdΔLrp4 mice exhibit a reduction in adipocyte hypertrophy and improved glucose and lipid homeostasis, marked by increased glucose and insulin tolerance and reduced serum fatty acids, and mirror the effect of sclerostin deficiency on whole-body metabolism. Indeed, epistasis studies place adipocyte-expressed Lrp4 and sclerostin in the same genetic cascade that regulates adipocyte function. Intriguingly, ObΔLrp4 mice, which exhibit dramatic increases in serum sclerostin, accumulate body fat and develop impairments in glucose tolerance and insulin sensitivity despite development of a high bone mass phenotype. These data indicate that expression of Lrp4 by both the adipocyte and osteoblast is required for normal sclerostin endocrine function and that the impact of sclerostin deficiency on adipocyte physiology is distinct from the effect on osteoblast function.

The comorbidity of obesity and osteopenia/osteoporosis illustrates the coordination of adipose and bone metabolism via endocrine communication and by common regulatory mechanisms. Adipose-derived hormones, like leptin and adiponectin, affect bone mass accrual through both direct and indirect effects on the osteoblast (1, 2), and recent advances have identified bone-specific factors that affect adipocyte hypertrophy and insulin sensitivity (3–5). Moreover, the fate specification of bipotential progenitors, present in the bone marrow and adipose stromal vascular fraction, to the osteoblastic and adipocytic lineages are reciprocally regulated by mitogen-activated protein kinase (6), bone morphogenetic (7), and Wnt/β-catenin signaling (8, 9).

Sclerostin, a cysteine knot glycoprotein, is a potent inhibitor of bone acquisition that antagonizes Wnt/β-catenin signaling (10, 11). Secreted primarily by bone matrix–embedded osteocytes, sclerostin binds the first β-propeller of the Wnt co-receptors low density lipoprotein receptor–related protein 5 (Lrp5) and Lrp6, expressed by osteoblasts and their progenitors. This interaction impedes recognition of Wnt1-class ligands by Lrp5/6 (12–14) and prevents the formation of the ternary Wnt:Frizzled:Lrp5/6 complex necessary for the initiation of β-catenin signals that drive osteoblast commitment and the attainment of a mature phenotype (15, 16).

We recently demonstrated that, in addition to its local actions in bone, sclerostin fulfils an endocrine function that regulates body composition and adipocyte metabolism. $Sost^{-/-}$ mice accumulate less body fat and exhibit an increase in insulin sensitivity in association with increased markers of Wnt/β-catenin signaling activation in adipose tissue depots and alterations in the ratio of anabolic to catabolic metabolism in adipocytes (3). Pharmacological inhibition of sclerostin activity with neutralizing antibodies produces an identical phenotype, whereas ectopic sclerostin overexpression stimulates adipocyte hypertrophy and impairs glucose homeostasis. These data accord with a growing number of studies that document a correlation between serum sclerostin levels and metabolic disease in humans. Serum sclerostin levels are increased in type 2 diabetics (17–19) and are positively associated with fat mass (20, 21) and tissue insulin resistance (22, 23).

Within the bone microenvironment, the anti-anabolic actions of sclerostin are facilitated by Lrp4, a member of the same protein family as Lrp5 and Lrp6 (24). Mice globally deficient of this receptor exhibit impairments in embryonic limb development and perinatal lethality, likely the result of Lrp4's function in neuromuscular junction formation (25, 26), but

This work was supported by Merit Review Awards BX003724 (to R. C. R.) and BX001234 (to T. L. C.) from the Biomedical Laboratory Research and Development Service of the Veterans Affairs Office of Research and Development and NIDDK, National Institutes of Health Grants DK099134 (to R. C. R.) and DK116746 (to M. J. W.). The authors declare that they have no conflicts of interest with the contents of this article. The content is solely the responsibility of the authors and does not necessarily represent the official views of the National Institutes of Health.

This article contains Figs. S1–S3 and Table S1.

[1] Recipient of a senior research career scientist award from the Department of Veterans Affairs.

[2] To whom correspondence should be addressed. Tel.: 410-502-6412; Fax: 443-287-4428; E-mail: rriddle1@jhmi.edu.

point mutations in the extracellular domain of human LRP4 (R1170W and W1186S) are associated with a bone overgrowth phenotype (27) reminiscent of that in sclerosteosis and van Buchem disease patients, who lack normal sclerostin protein production (28–30). Direct interaction of Lrp4 and sclerostin was confirmed in an MS screen by Leupin *et al.* (27), who also demonstrated that genetic knockdown of the receptor *in vitro* ablated sclerostin's inhibitory effect on osteoblast differentiation. Likewise, targeted ablation of Lrp4 expression in the osteoblast lineage (31, 32) or pharmacological inhibition of the Lrp4:sclerostin interaction *in vivo* (31) dramatically increases bone formation and bone mass.

In this study, we explored the contribution of Lrp4 to sclerostin's endocrine function by ablating its expression in adipose tissue and bone. Similar to its role in facilitating sclerostin function in bone, inhibiting Lrp4 function in adipocytes abolished sclerostin's ability to enhance adipogenesis *in vitro* and resulted in a reduction in adipocyte hypertrophy and improved insulin sensitivity *in vivo*. Loss of Lrp4 function in osteoblasts leads to sclerostin overexpression and the opposite metabolic phenotype. Collectively, these data indicate that Lrp4 expressed by adipocytes and osteoblasts regulates normal sclerostin endocrine function by affecting its activity and expression, respectively.

Results

Lrp4 is required for sclerostin to enhance in vitro adipocyte differentiation

The ability of osteocyte-produced sclerostin to inhibit osteoanabolic Wnt signaling is facilitated by its interaction with the Lrp4 receptor expressed by osteoblasts and their progenitors (27, 32). Because Lrp4 is expressed in adipose tissue (Fig. 1, *A* and *B*) and by adipocytes induced to differentiation *in vitro* (Fig. 1*C*), we predicted that Lrp4 also contributes to the metabolic actions of sclerostin. As a first step in testing this hypothesis, stromal vascular cells were isolated from the inguinal fat pads of mice containing $Lrp4^{flox}$ alleles and infected with an adenovirus encoding Cre recombinase to abolish Lrp4 expression (ΔLrp4, Fig. 1*D*) or GFP as a control. Cells were then cultured under adipogenic conditions in the presence of vehicle or recombinant mouse sclerostin (rScl).[3]

Consistent with our previous report (3), rScl treatment inhibited the expression of the Wnt target gene Axin2 (33) (Fig. 1*D*) and enhanced the adipogenic differentiation of control cells, as indexed by histochemical staining for accumulated lipids (Fig. 1*F*) and qPCR analysis of Cebpa, Fabp4, Lpl, and Pparg mRNA levels (Fig. 1*G*). ΔLrp4 adipocytes exhibited increases in Axin2 mRNA (Fig. 1*D*) and β-catenin protein levels (Fig. 1*E*) and impairment in differentiation and were strikingly resistant to rScl treatment, which was unable to enhance lipid accumulation or the expression of adipocyte markers. A similar effect of Lrp4 loss of function was observed when radiolabeled tracers were used to assess adipocyte metabolism *in vitro*. Although rScl increased *de novo* fatty acid synthesis (Fig. 1*H*), suppressed fatty acid oxidation (Fig. 1*J*), and induced coordinate changes in anabolic and catabolic gene expression (Fig. 1, *I* and *K*) in control adipocytes, ΔLrp4 adipocytes were unaffected by rScl treatment. Importantly, loss of Lrp4 function did not affect the expression Dkk1, Sostdc1, and Agrin or the ability of Dkk1 to enhance adipocyte differentiation (Fig. S1). Thus, Lrp4 is required for sclerostin to enhance adipocyte differentiation *in vitro*.

AdΔLrp4 mice have small adipocytes and improved glucose metabolism

To determine the role of Lrp4 in adipocytes *in vivo*, we crossed $Lrp4^{flox}$ mice with AdipoQ-Cre mice (34) to generate mice in which Lrp4 expression was ablated specifically in white and brown adipose tissue (AdΔLrp4, Figs. 1*B* and 2*A*). AdΔLrp4 mice were born at the expected Mendelian ratios (data not shown) and had normal body weight (Fig. 2*B*), serum sclerostin levels (Fig. 2*C*), and bone volume (Fig. S2). In agreement with Lrp4's role as a facilitator of Wnt signaling antagonism in bone, Axin2 expression (Fig. 2*D*) and β-catenin protein levels (Fig. 2*E*) were increased in the white adipose tissue of the mutant mice relative to controls.

We expected that the increase in Wnt signaling in white adipocytes of AdΔLrp4 mice would lead to the development of a lean phenotype similar to that observed in $Sost^{-/-}$ mice (3), but whole-body fat mass and the weights of individual fat pads in AdΔLrp4 were comparable with control littermates (Fig. 2, *F–H*). However, histological analysis of adipocyte morphology in both the gonadal and inguinal fat pads revealed significant reductions in adipocyte size in AdΔLrp4 mice relative to controls that led to an increase in adipocyte numbers per field (Fig. 2, *I–L*). The modest down-regulation of genes associated with adipocyte differentiation (Fig. 2*M*) together with alteration of genes involved in fatty acid synthesis and lipid catabolism (Fig. 2, *N* and *O*) suggest that the reduced adipocyte size is at least partially due to an inhibition of adipocyte hypertrophy and changes in the ratio of anabolic to catabolic metabolism. The maintenance of normal fat pad weights in Lrp4 mutant mice is likely due to an increase in proliferation and the accumulation of small adipocytes, as Ki67 staining in the stromal vascular fraction (Fig. 2*P*), fat pad DNA content (Fig. 2*Q*), and Ccnd1 expression were increased (Fig. 2*R*), whereas the mRNA levels of cyclin-dependent kinase inhibitors were reduced in adipose tissue relative to controls. The expression of Dkk1 and Sostdc1 was not affected by loss of Lrp4 function in white adipose tissue (Fig. S1), and the morphology of brown adipose tissue and liver was identical in control and mutant mice (Fig. S2).

Further analysis of AdΔLrp4 mice revealed an improvement in glucose metabolism. Although the blood glucose levels of randomly fed mice were normal (Fig. 3*A*), mutant mice exhibited a significant reduction in serum insulin (Fig. 3*B*), which is usually indicative of an increase in insulin sensitivity. In line with this idea, the mutants performed better in glucose tolerance tests (Fig. 3, *C* and *D*) and insulin tolerance tests (Fig. 3, *E* and *F*). The increase in insulin sensitivity is likely to be driven, at least in part, by changes in adipose tissue sensitivity, as insulin-stimulated Akt phosphorylation was increased in the inguinal fat pads of the mutants (Fig. 3, *G* and *H*), and serum free fatty acid levels were reduced (Fig. 3*J*) without a change in serum

[3] The abbreviations used are: rScl, recombinant mouse sclerostin; qPCR, quantitative PCR; qNMR, quantitative NMR; BW, body weight; WAT, white adipose tissue; GTT, glucose tolerance test; ITT, insulin tolerance test.

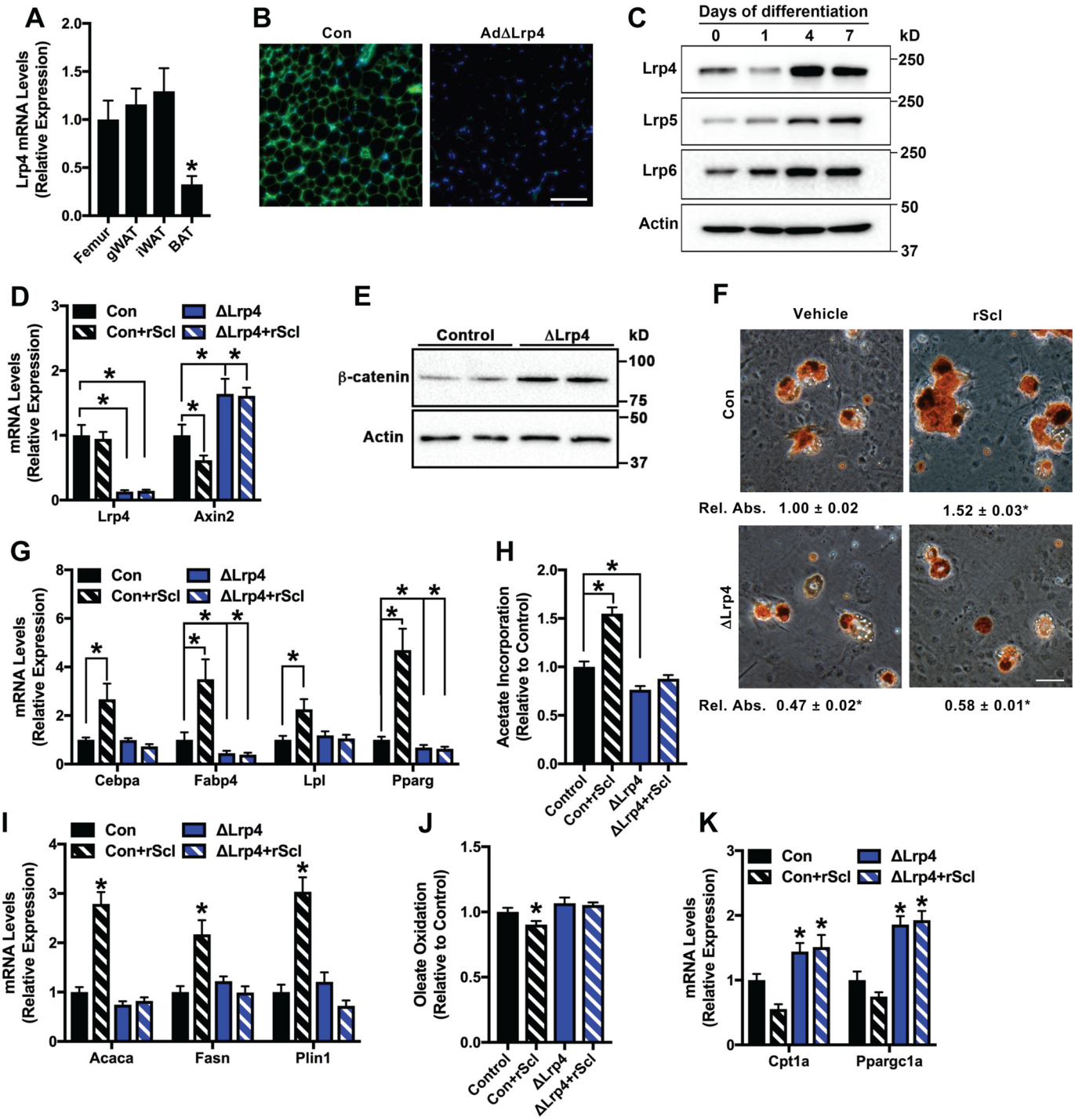

Figure 1. Lrp4 mediates the adipogenic effects of sclerostin *in vitro*. *A*, qPCR analysis of Lrp4 expression in the femur, gonadal WAT (*gWAT*), inguinal WAT (*iWAT*), and brown adipose tissue. *B*, immunohistochemical detection of Lrp4 expression in inguinal adipose tissue of control (*Con*) and AdΔLrp4 mice. *C*, Western blot analysis of Lrp4, Lrp5, and Lrp6 expression during *in vitro* adipogenic differentiation of stromal vascular cells isolated from iWAT. *D*, qPCR analysis of Lrp4 and Axin2 mRNA levels in control and ΔLrp4 adipocyte cultures treated with vehicle or rScl for 7 days. *E*, Western blot analysis of β-catenin protein levels in control and ΔLrp4 adipocytes. *F*, Oil Red O staining of primary adipocyte cultures treated with vehicle or recombinant mouse sclerostin; ×20 magnification. Relative absorbance (*Rel. Abs.*) was calculated after stain extraction. *G*, qPCR analysis of markers of adipocyte differentiation. *H*, relative *de novo* lipogenesis measured by the incorporation of [^{3}H]acetate into cellular lipids. *I*, qPCR analysis of enzymes involved in fatty acid synthesis. *J*, relative oleate oxidation measured by the conversion of [1-^{14}C]oleic acid to $^{14}CO_2$. *K*, qPCR analysis of Cpt1a and Ppargc1a mRNA levels. *In vitro* studies were repeated in at least two independent experiments (n = 6–9 replicates). All data are represented as mean ± S.E. *, $p < 0.05$ *versus* control unless otherwise indicated. *Scale bar* = 200 μm.

triglyceride levels (Fig. 3*I*). Serum levels of leptin, adiponectin, and osteocalcin were similar in control and mutant mice (Table S1). The metabolic phenotype of female AdΔLrp4 mice mirrored that of male mutants (Fig. S3). Therefore, adipocyte-specific Lrp4 mutants partially phenocopy the metabolic effects of sclerostin deficiency (3) and raise the possibility that Lrp4 mediates at least some of sclerostin's endocrine function in white adipose tissue.

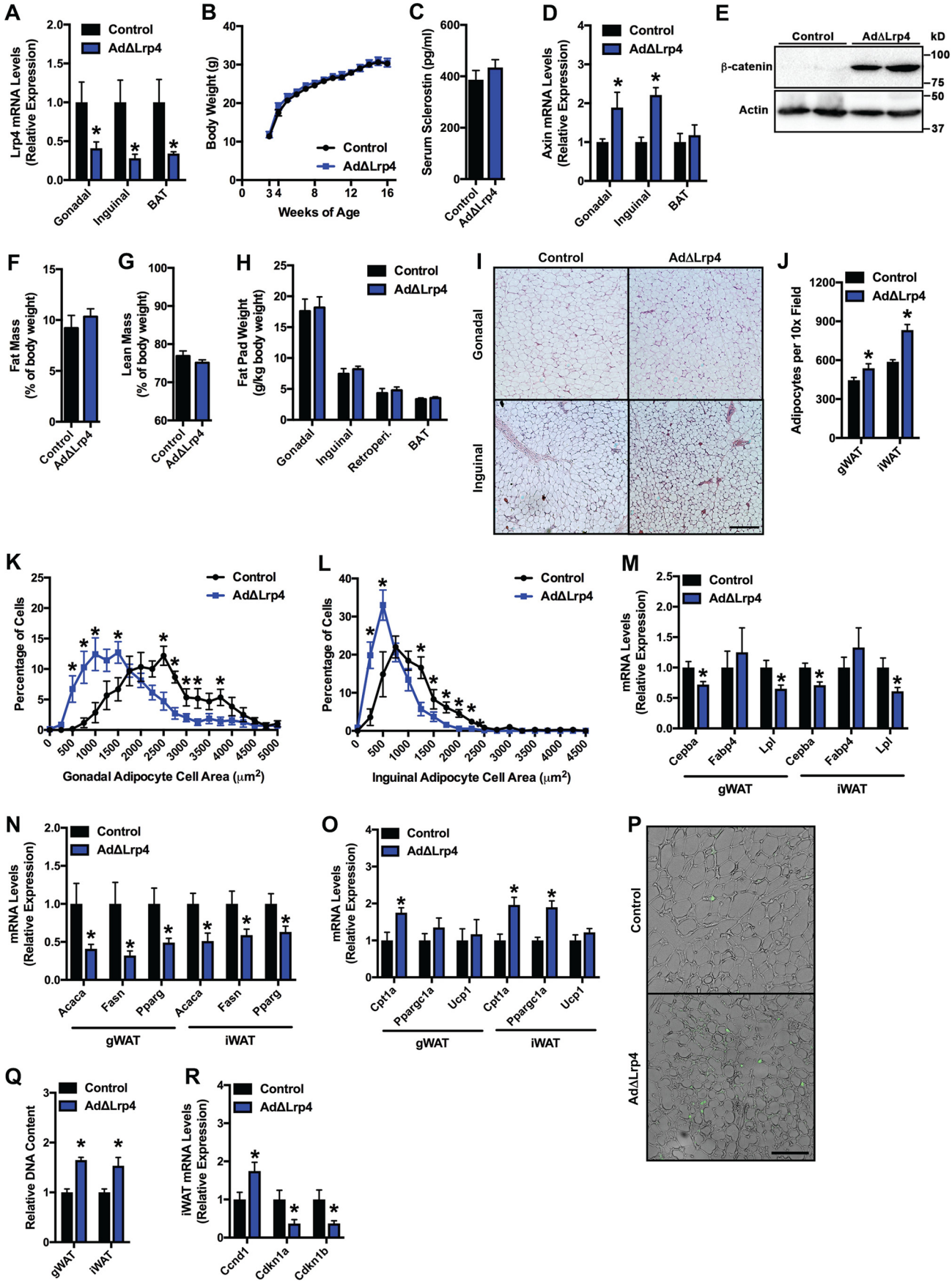
A
Lrp4 mRNA Levels (Relative Expression)
Control
AdΔLrp4
Gonadal
Inguinal
BAT
B
Body Weight (g)
Weeks of Age
C
Serum Sclerostin (pg/ml)
D
Axin mRNA Levels (Relative Expression)
E
Control
AdΔLrp4
kD
β-catenin
Actin
100
75
50
37
F
Fat Mass (% of body weight)
G
Lean Mass (% of body weight)
H
Fat Pad Weight (g/kg body weight)
Retroperi.
I
Gonadal
Inguinal
J
Adipocytes per 10x Field
gWAT
iWAT
K
Percentage of Cells
Gonadal Adipocyte Cell Area (μm²)
L
Inguinal Adipocyte Cell Area (μm²)
M
mRNA Levels (Relative Expression)
Cepba
Fabp4
Lpl
N
Acaca
Fasn
Pparg
O
Cpt1a
Ppargc1a
Ucp1
P
Q
Relative DNA Content
R
iWAT mRNA Levels (Relative Expression)
Ccnd1
Cdkn1a
Cdkn1b

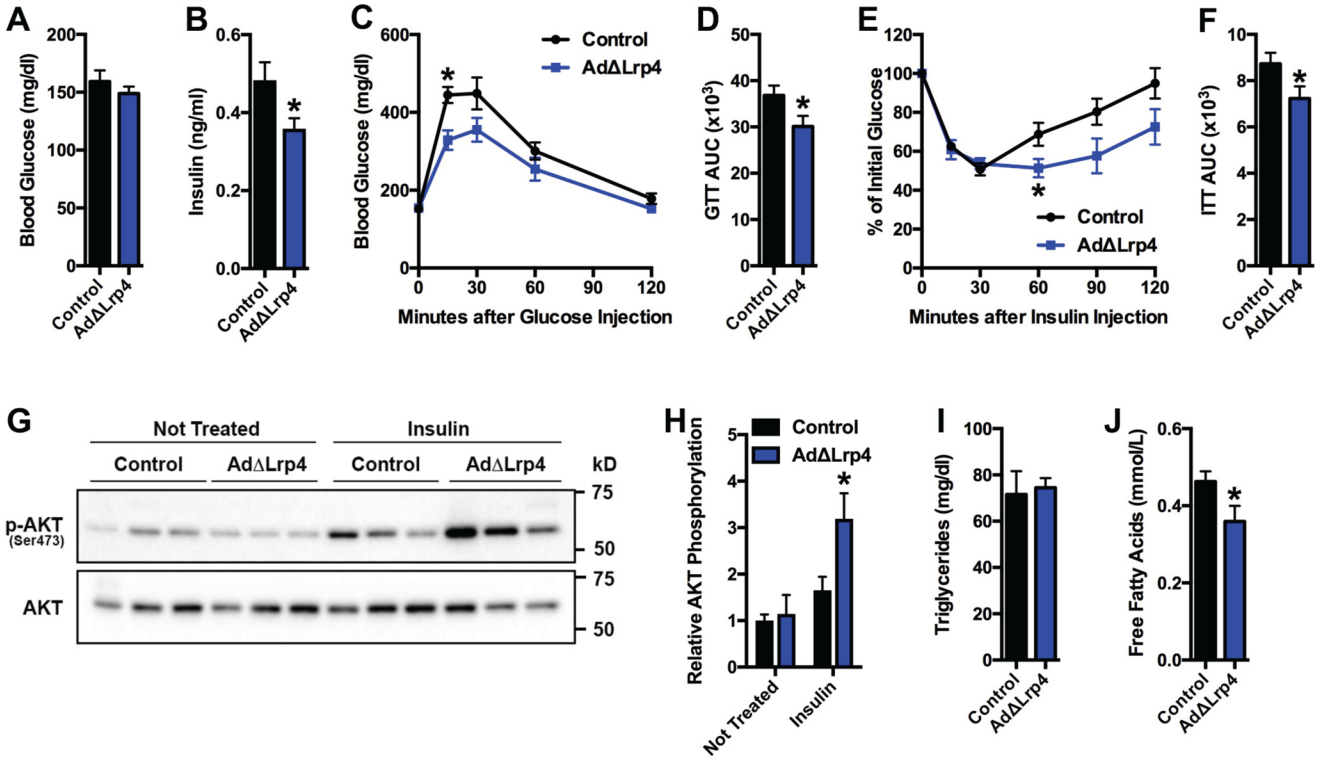

Figure 3. Loss of Lrp4 function in adipocytes affects glucose and lipid metabolism. *A*, glucose levels in randomly fed 16-week-old male control and AdΔLrp4 mice ($n = 10$ mice/group). *B*, insulin levels in randomly fed mice ($n = 8$ mice/group). *C* and *D*, glucose tolerance test (GTT) and area under the curve (*AUC*) analysis ($n = 8$–9 mice/group). *E* and *F*, insulin tolerance test (*ITT*) and area under the curve analysis ($n = 7$–8 mice/group). *G* and *H*, Western blot analysis and quantification of Akt phosphorylation in inguinal adipose tissue before and after insulin stimulation ($n = 6$ mice/group). *I* and *J*, serum triglyceride and free fatty acid levels in randomly fed control and AdΔLrp4 mice ($n = 10$ mice/group). All data are represented as mean ± S.E. *, $p < 0.05$.

Epistasis reveals a genetic interaction between adipocyte-expressed Lrp4 and sclerostin

As a genetic test of the interaction between sclerostin and Lrp4 in adipocytes, we performed an epistasis study by crossing AdΔLrp4 mice with Sost$^{+/-}$ mice to generate cohorts of compound heterozygous mice lacking one allele of the *Sost* gene globally and one allele of *Lrp4* in adipocytes (AdΔLrp4/$^{+}$; Sost$^{+/-}$) as well as the appropriate heterozygous controls (Sost$^{+/-}$ and AdΔLrp4/$^{+}$; see "Experimental procedures" for the breeding strategy). In support of the notion that sclerostin and adipocyte-expressed Lrp4 work in concert to regulate adipose tissue metabolism, compound heterozygous mice exhibited an increase in Axin2 expression (Fig. 4*A*) even though serum sclerostin levels were reduced by only 30% (Fig. 4*B*). More importantly, the compound mutants developed reductions in both whole-body fat mass and the weights of the gonadal and inguinal fat pads, whereas the body weight remained normal (Fig. 4, *C–F*). Within white adipose tissue depots, adipocyte size (Fig. 4, *G* and *H*) was reduced in compound heterozygotes relative to controls and was accompanied by changes in metabolic gene expression that were similar to the genetic ablation of both Lrp4 alleles in adipocytes (Fig. 4*I*). An increase in the abundance of multilocular adipocytes was also evident in compound heterozygotes, raising the possibility of an increase in the browning of this tissue. In all cases, Sost$^{+/-}$ and AdΔLrp4/$^{+}$ mice were similar to controls.

The compound heterozygous mice also mirrored the improvements in glucose metabolism evident here in AdΔLrp4 mice (Fig. 3) and previously in Sost$^{-/-}$ mice (3). Blood glucose levels of randomly fed mice were comparable with controls, but serum insulin levels were significantly reduced in compound heterozygotes (Fig. 4, *J* and *K*). Similarly, glucose tolerance (Fig. 4, *L* and *M*) and insulin tolerance (Fig. 4, *N* and *O*) were increased in compound heterozygous mice, which also had significantly lower serum free fatty acid levels (Fig. 4, *P* and *Q*). Sost$^{+/-}$ and AdΔLrp4/$^{+}$ mice were indistinguishable from controls in all of these measures. Taken together, these results

Figure 2. Loss of Lrp4 function alters adipocyte physiology. *A*, qPCR analysis of Lrp4 mRNA levels in gonadal, inguinal, and intrascapular brown adipose tissue ($n = 6$ mice/group). *B*, body weight was assessed weekly ($n = 10$ mice/group). *C*, serum sclerostin levels in 16 week-old-male control and AdΔLrp4 mice ($n = 8$ mice/group). *D*, qPCR analysis of Axin2 expression in the fat pads of control and AdΔLrp4 mice ($n = 6$ mice/group). *E*, Western blot analysis of β-catenin protein levels in the inguinal fat pads of control and AdΔLrp4 mice. *F* and *G*, qNMR analysis of fat mass and lean mass ($n = 8$ mice). *H*, adipose depot weights of 16-week-old male control and AdΔLrp4 mice ($n = 6$–7 mice). *I*, representative histological sections of the gonadal and inguinal fat pads; ×10 magnification. *J*, quantification of adipocyte number per ×10 magnified field ($n = 6$–7 mice). *K* and *L*, frequency distribution of adipocyte size in the gonadal and inguinal fat pads ($n = 6$–7 mice). *M–O*, qPCR analysis of genes associated with adipocyte differentiation, *de novo* fatty acid synthesis, fatty acid catabolism, and adipose tissue browning. *P*, Ki67 immunostaining in the inguinal fat pads of control and AdΔLrp4 mice. Merged FITC and bright-field images are shown. *Q*, relative DNA content in the gonadal and inguinal fat pads ($n = 4$–5 mice). *R*, qPCR analysis of cell cycle regulator expression in the inguinal fat pads of control and AdΔLrp4 mice ($n = 6$ mice/group). All data are represented as mean ± S.E. *, $p < 0.05$. *Scale bars* = 200 μm.

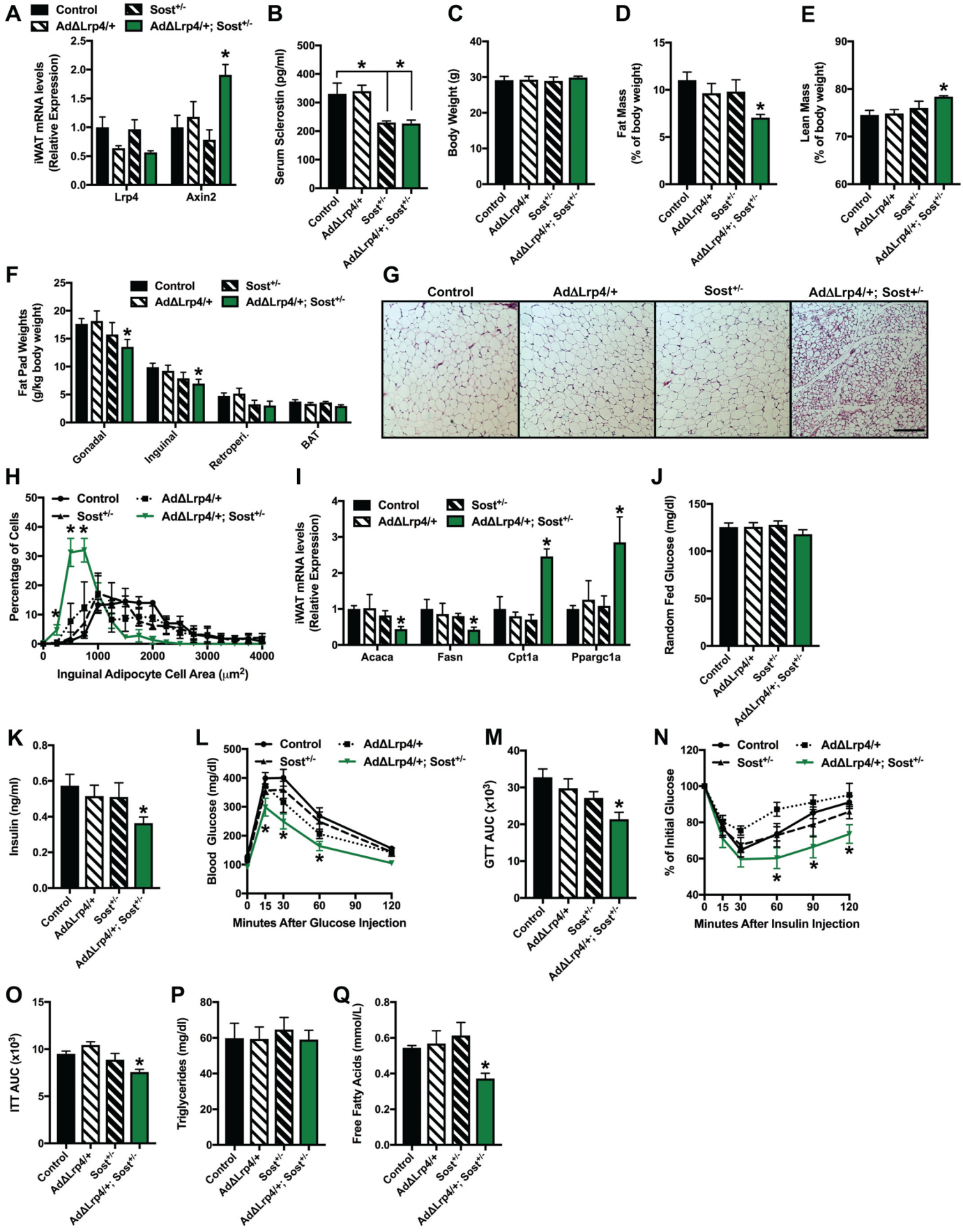
A
Control
Sost+/-
AdΔLrp4/+
AdΔLrp4/+; Sost+/-
iWAT mRNA levels (Relative Expression)
Lrp4
Axin2
B
Serum Sclerostin (pg/ml)
C
Body Weight (g)
D
Fat Mass (% of body weight)
E
Lean Mass (% of body weight)
F
Fat Pad Weights (g/kg body weight)
Gonadal
Inguinal
Retroperi.
BAT
G
Control
AdΔLrp4/+
Sost+/-
AdΔLrp4/+; Sost+/-
H
Percentage of Cells
Inguinal Adipocyte Cell Area (μm2)
I
iWAT mRNA levels (Relative Expression)
Acaca
Fasn
Cpt1a
Ppargc1a
J
Random Fed Glucose (mg/dl)
K
Insulin (ng/ml)
L
Blood Glucose (mg/dl)
Minutes After Glucose Injection
M
GTT AUC (x10³)
N
% of Initial Glucose
Minutes After Insulin Injection
O
ITT AUC (x10³)
P
Triglycerides (mg/dl)
Q
Free Fatty Acids (mmol/L)

provide strong genetic evidence that Lrp4 facilitates sclerostin's function in fat in a manner analogous to that in bone.

Lrp4 deficiency in adipocytes alters Bmp signaling

Because alterations in sclerostin function in adipocytes produce coordinate changes in Bmp signaling, and administration of noggin inhibits the effect of rScl on adipocyte differentiation *in vitro* (3), we predicted that the loss of Lrp4 expression would decrease the activation of this adipogenic pathway (35). Consistent with our hypothesis, Bmp4 mRNA expression levels and the phosphorylation of Smad1/5/9 were reduced in the inguinal fat pads of AdΔLrp4 mice (Fig. 5, *A* and *B*). Likewise, although rScl increased the expression of Bmp4 in *in vitro* cultures of control adipocytes, expression was reduced in ΔLrp4 cells and unresponsive to exogenous sclerostin (Fig. 5*C*).

To ensure that regulation of Bmp4 was indeed downstream of Lrp4 in the control of adipogenesis, we next treated differentiating control and ΔLrp4 adipocytes with recombinant Bmp4. Bmp4 treatment enhanced *in vitro* adipogenesis in control cultures, which was marked by an increase in Oil Red O staining and an increase in adipogenic gene expression (Fig. 5, *D* and *E*). Importantly, ΔLrp4 cultures were fully responsive to Bmp4 treatment, which was able to rescue the defect in adipogenesis associated with Lrp4 loss of function. Similarly, Bmp4 increased fatty acid synthesis (Fig. 5*F*) and affected the expression of metabolic genes in both control and ΔLrp4 cultures (Fig. 5, *G* and *H*) and, in both cases, reversed the changes induced by Lrp4 deficiency. Therefore, alterations in Bmp4 expression and activity similar to those evident in Sost$^{-/-}$ mice (3) appear to underlie the differentiation and metabolic defects associated with Lrp4 deficiency in adipocytes.

ObΔLrp4 mice overproduce sclerostin and accumulate adipose tissue

Although the loss of Lrp4 function in the osteoblast lineage increases bone mass, it also leads to the overexpression of Sost via an unknown compensatory mechanism (31, 32). We questioned whether this deregulation of sclerostin expression would, in turn, lead to alterations in body composition and metabolism by generating cohorts of male osteoblast/osteocyte-specific Lrp4 mutants (Lrp4^{flox}; Ocn-Cre, ObΔLrp4) and control littermates.

As reported previously (31, 32), ablation of Lrp4 expression in osteoblasts and osteocytes (Fig. 6*A*) increased bone volume (Fig. 6, *C* and *D*) and induced a more than 4-fold increase in serum sclerostin levels (Fig. 6*B*). Analysis of Sost mRNA levels in the femur indicated that the increase in serum abundance is at least partially due to increased expression (Fig. 6*A*). ObΔLrp4 mice maintained normal body weight (Fig. 6*E*), but, consistent with the idea that sclerostin favors adipose tissue accumulation via an endocrine mechanism, the mutants exhibited significant increases in whole-body fat mass (Fig. 6*F*) and the weight of white adipose tissue depots (Fig. 6*H*) and a reduction in lean tissue mass (Fig. 6*G*). Additionally, osteoblast-specific mutants exhibited a significant increase in adipocyte hypertrophy in the gonadal and inguinal fat pads (Fig. 6, *I* and *J*), coincident with a reduction in Wnt target gene expression and increased expression of genes involved in *de novo* fatty acid synthesis (Fig. 6*K*).

Glucose and lipid metabolism were also negatively affected by Lrp4 deficiency in osteoblasts and osteocytes and the resulting overproduction of sclerostin. Randomly fed ObΔLrp4 mice were hyperglycemic (Fig. 6*L*) and hyperinsulinemic (Fig. 6*M*) compared with control littermates and performed poorly in standard glucose tolerance (Fig. 6, *N* and *O*) and insulin tolerance tests (Fig. 6, *P* and *Q*). Serum triglyceride levels (Fig. 6, *R* and *S*) were also elevated in osteoblast/osteocyte-specific mutants, suggesting development of dyslipidemia, but serum leptin, adiponectin, and undercarboxylated osteocalcin were similar in control and mutant mice (Table S1). The increase in total osteocalcin levels evident in osteoblast-specific mutants likely reflects the increase in bone formation. Therefore, Lrp4 expression by osteoblasts and osteocytes also appears to be essential for normal sclerostin endocrine action, likely as a result of the requirement for the receptor to maintain sclerostin expression levels within the normal range.

Discussion

Down-regulation of Wnt/β-catenin signaling is a key step in the commitment of progenitor cells to the adipogenic lineage and attainment of a mature adipocyte phenotype (8, 36, 37). In our previous work (3), we demonstrated that bone-derived sclerostin, which had been viewed previously only as a local inhibitor of bone formation (28, 38), acts as an endocrine factor that promotes adipogenesis and adipocyte hypertrophy in association with the inhibition of Wnt signaling in white adipose tissue. In this study, we used a series of *in vitro* and *in vivo* approaches to determine the contribution of Lrp4 to sclerostin's endocrine actions in fat. As noted above, this receptor directly interacts with sclerostin in the bone microenvironment and thereby facilitates sclerostin's ability to antagonize the recognition of Wnt ligands by Lrp5/6 in the osteoblast and inhibit bone formation (27, 31, 32).

Lrp4 is well-expressed by white adipocytes, with mRNA levels commensurate with those found in bone, and it appears to function in a manner analogous to that described in osteoblasts. Our *in vitro* experiments demonstrated that ablating Lrp4 expression produces a defect in the adipogenic differentiation of stromal vascular cells (which could be due to the presence of sclerostin in the serum used during *in vitro* culture) and renders

Figure 4. Sclerostin and adipocyte-expressed Lrp4 are in the same genetic cascade. *A*, qPCR analysis of Lrp4 and Axin2 mRNA levels in the inguinal fat pads of 16-week-old control, Sost$^{+/-}$, AdΔLrp4/+, and AdΔLrp4/+; Sost$^{+/-}$ mice (n = 5–6 mice/group). *B*, serum sclerostin levels (n = 7–10 mice/group). *C*, body weights at 16 weeks of age (n = 7–10 mice/group). *D* and *E*, qNMR analysis of fat mass and lean mass (n = 7–10 mice/group). *F*, adipose depot weights of 16-week-old male mice (n = 7–10 mice/group). *G* and *H*, representative histological sections (×10 magnification) and frequency distribution of adipocyte size in inguinal fat pads (n = 7–10 mice/group). *I*, qPCR analysis of genes involved in *de novo* fatty acid synthesis and fatty acid catabolism (n = 5–6 mice/group). *J*, glucose levels in randomly fed mice (n = 7–10 mice/group). *K*, insulin levels in randomly fed mice (n = 7–10 mice/group). *L* and *M*, GTT and area under the curve (*AUC*) analysis (n = 7–10 mice/group). *N* and *O*, ITT and area under the curve analysis (n = 7–10 mice/group). *P* and *Q*, serum triglyceride and free fatty acid levels in randomly fed control and AdΔLrp4 mice (n = 7–10 mice/group). All data are represented as mean ± S.E. *, $p < 0.05$. *Scale bar* = 200 μm.

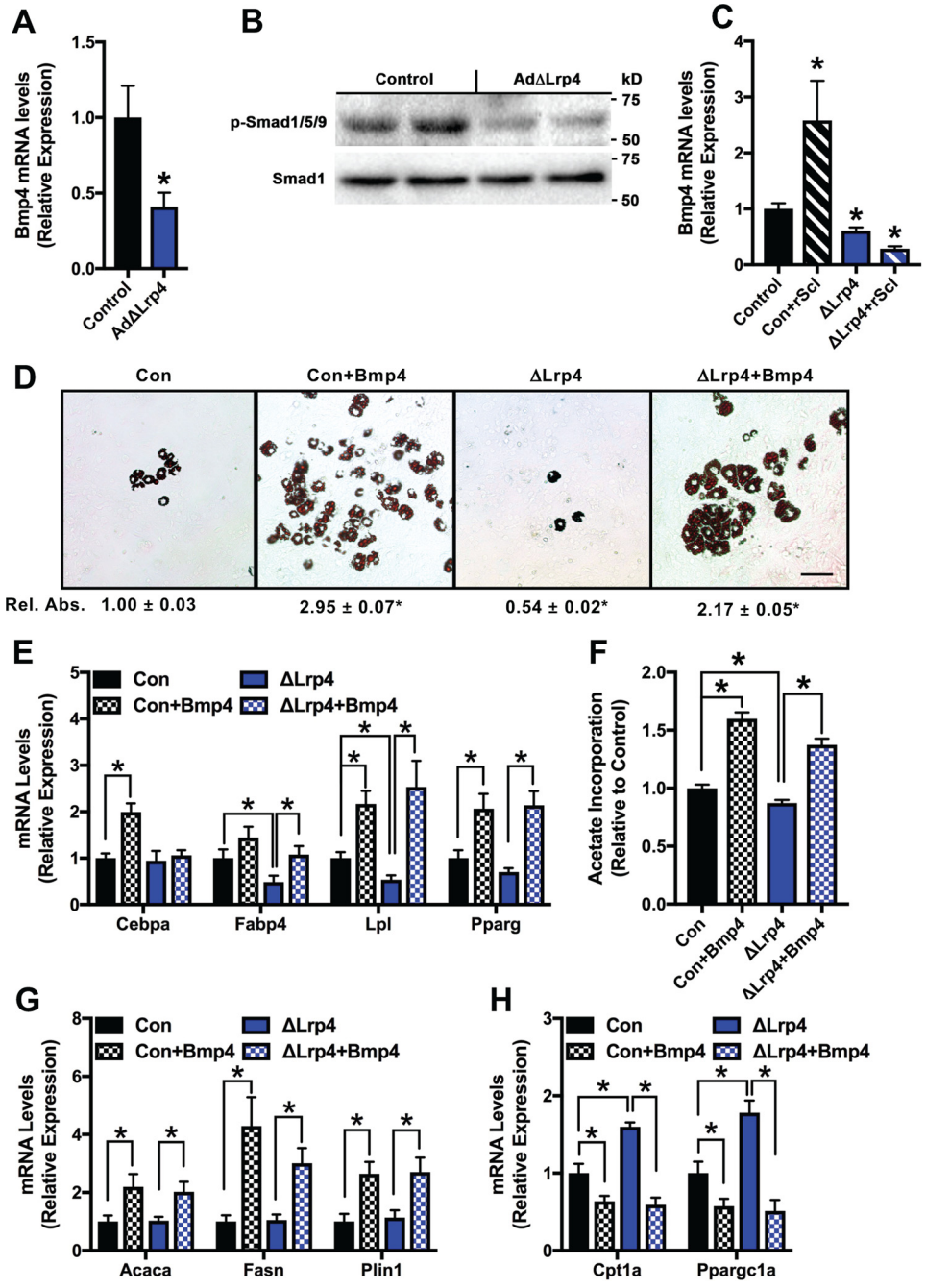

Figure 5. Bmp signaling is reduced in Lrp4-deficient adipocytes. *A*, qPCR analysis of Bmp4 mRNA levels in iWAT of 16-week-old control and AdΔLrp4 mice ($n = 6$ mice/group). *B*, immunoblot analysis of phosphorylated Smad1/5/9 levels in iWAT (results are representative of blots for $n = 6$ mice/group). *C*, qPCR analysis of Bmp4 mRNA levels in control (*Con*) and ΔLrp4 adipocyte cultures treated with vehicle or rScl for 7 days. *D*, Oil Red O staining of primary adipocyte cultures treated with vehicle or recombinant Bmp4; ×20 magnification. Relative absorbance (*Rel. Abs.*) was calculated after stain extraction. *E*, qPCR analysis of markers of adipocyte differentiation. *F*, relative *de novo* lipogenesis measured by incorporation of [^{3}H]acetate into cellular lipids. *G*, qPCR analysis of enzymes involved in fatty acid synthesis. *H*, qPCR analysis of Cpt1a and Ppargc1a mRNA levels. *In vitro* studies were repeated in at least two independent experiments ($n = 6$–12 replicates). All data are represented as mean ± S.E. *, $p < 0.05$. *Scale bar* = 200 μm.

adipocytes resistant to the effects of recombinant sclerostin on both adipogenesis and the ratio of catabolic to anabolic metabolism. Importantly, the adipogenic effects of Dkk1, which may also interact with Lrp4 (39), remained intact, and the mRNA levels of other interacting proteins remained largely normal. The metabolic phenotype of mice lacking Lrp4 in adipocytes partially mirrors that of Sost$^{-/-}$ mice (3). Both mutants exhibit an increase in markers of Wnt signaling in white adipose tissue, reduction in adipocyte size, and improvements in insulin sensitivity that were at least partially driven by an increase in the sensitivity of the adipocyte. The development of these phenotypes also appears to be secondary to modifications in the same pathway, as both AdΔLrp4 and Sost$^{-/-}$ mice exhibited reductions in Bmp4 expression and Smad phosphorylation, which has been reported previously to induce adipocyte hypertrophy by stimulating fatty acid synthesis (35). Further, our genetic epistasis experiment places Lrp4 and sclerostin in the same genetic pathway that regulates adipocyte physiology.

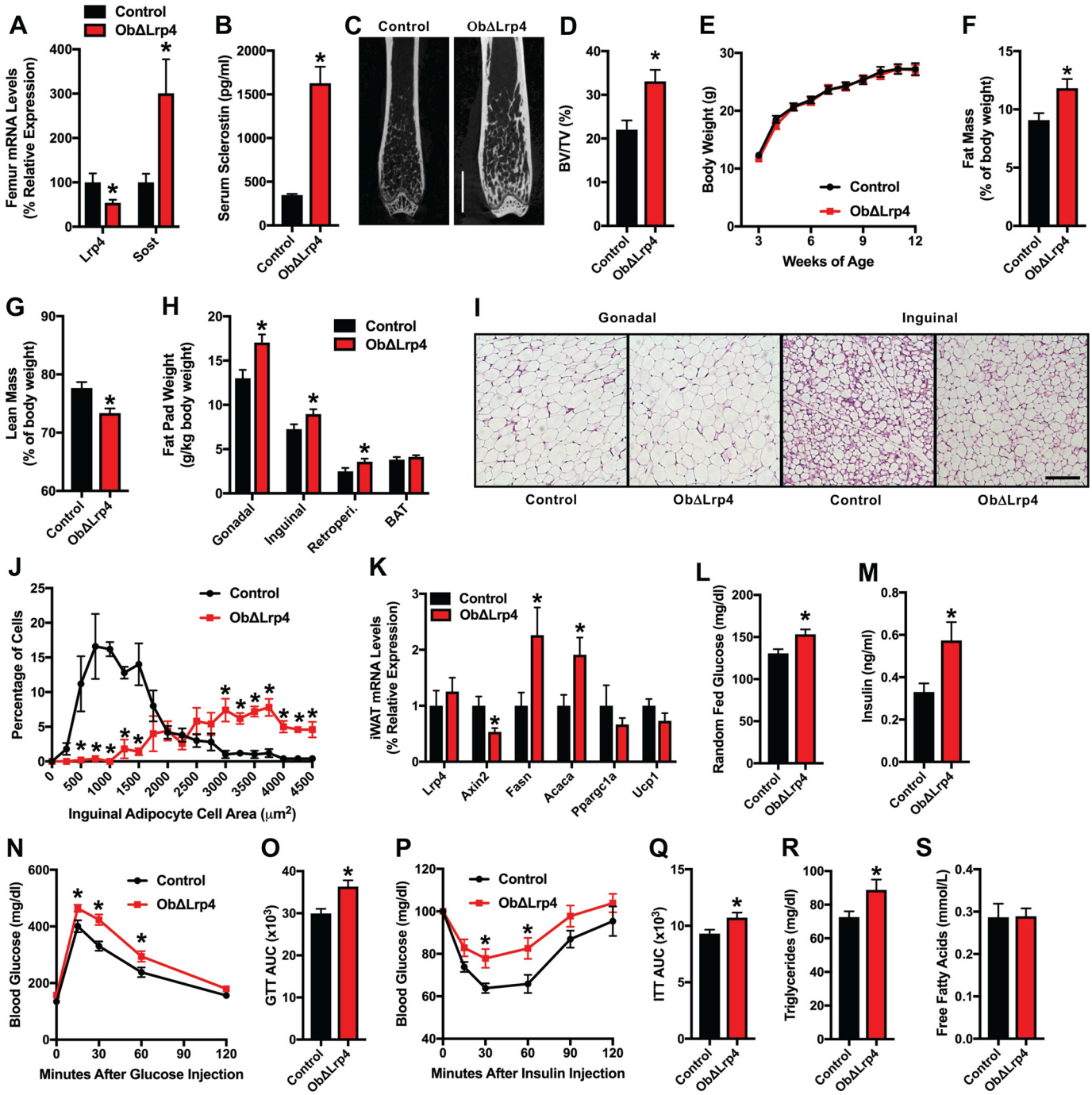

Figure 6. Loss of Lrp4 function in the osteoblast increases sclerostin expression and fat mass. *A*, qPCR analysis of Lrp4 and Sost mRNA levels in the femur of 12 week old control and ObΔLrp4 mice ($n = 8$ mice/group). *B*, serum sclerostin levels ($n = 8$ mice/group). *C* and *D*, representative Micro-computed tomography images and quantification of trabecular bone volume per tissue volume (*BV/TV*) in the distal femur ($n = 5$ mice/group). *Scale bar* = 2 mm. *E*, body weight was assessed weekly ($n = 10$–11 mice/group). *F* and *G*, qNMR analysis of fat mass and lean mass ($n = 9$–13 mice/group). *H*, adipose depot weights at 12weeks of age ($n = 11$–12 mice/group). *I*, representative histological sections of the gonadal and inguinal fat pads; ×10 magnification. *Scale bar* = 200 μm. *J*, frequency distribution of adipocyte size in inguinal fat pads ($n = 5$ mice). *K*, qPCR analysis of gene expression in inguinal fat pads ($n = 6$ mice/group). *L*, glucose levels in randomly fed mice ($n = 12$–13 mice/group). *M*, insulin levels in randomly fed mice ($n = 8$ mice/group). *N* and *O*, GTT and area under the curve (*AUC*) analysis ($n = 12$–13 mice/group). *P* and *Q*, ITT and area under the curve analysis ($n = 9$–10 mice/group). *R* and *S*, serum triglyceride and free fatty acid levels in randomly fed control and AdΔLrp4 mice ($n = 8$ mice/group). All data are represented as mean ± S.E. *, $p < 0.05$.

We expected that AdΔLrp4 mice would exhibit the decrease in adipose tissue mass evident in Sost$^{-/-}$ mice, but assessment of body composition by qNMR analysis and at necropsy revealed that the fat mass is equivalent in Lrp4 mutants and their control littermates. Our histological experiments suggest that the mutants are able to maintain normal fat mass by accumulating small adipocytes, likely through a compensatory increase in proliferation in the stromal vascular compartment and, potentially, subsequent commitment to the adipocyte lineage. Additional studies, including lineage tracing, will be required to more fully evaluate the impact of sclerostin and Lrp4 on the proliferation and differentiation of cells in this

compartment. Because Lrp4 expression increases during the differentiation process, these findings clearly indicate that Lrp4 facilitates the effects of sclerostin on adipocyte hypertrophy. However, we cannot rule out a possible role of sclerostin and Lrp4 in adipocyte specification because the AdipoQ-Cre transgene we utilized primarily drives recombination in mature adipocytes and does not impact the stromal vascular compartment that contains progenitor cells (40, 41). Examining the interaction of sclerostin and Lrp4 at this earlier stage of differentiation will require additional studies using stage-specific Cre lines and lineage tracing.

A surprising finding in this study is the lack of an effect of genetic ablation of Lrp4 in adipocytes on serum sclerostin levels. Most endocrine interactions are associated with feedback loops wherein the level of signaling in the target tissue influences the production and release of the endocrine factor. According to this paradigm, loss of Lrp4 function in adipocytes would be expected to increase sclerostin production and, perhaps, indirectly impact skeletal homeostasis. Our data indicate that, in mice fed a chow diet, signals downstream of the sclerostin:Lrp4 interaction do not signal back to bone. It remains to be seen whether signaling from adipocytes regulates sclerostin production under obesogenic conditions, but the recent observation that PPARγ contributes to the regulation of sclerostin expression in osteocytes could represent a potential mechanism (42).

The increase in sclerostin serum levels following genetic ablation of Lrp4 in the osteoblast lineage is consistent with previous studies (31, 32) suggesting a sclerostin chaperone action for Lrp4 that retains the protein within the bone microenvironment because an increase in expression was not observed. Our study suggests that the sclerostin:Lrp4 interaction may also induce feedback inhibition of sclerostin expression in the osteocyte, as Sost mRNA levels were increased in the femoral bone of osteoblast-specific mutants. The discrepancy between our findings and those of Chang *et al.* (31) could be due to the age or genetic background of the mice. Nonetheless, loss of Lrp4 function in the osteoblast is sufficient to alter body composition and phenocopy the effects of Adeno-associated virus-mediated Sost overproduction (3), which include accumulation of white adipose tissue and development of impaired glucose homeostasis. Thus, expression of Lrp4 by two cell types, the osteoblast and the adipocyte, is required for normal sclerostin endocrine actions.

The phenotypes of these mutant mice are also informative regarding the interactions of sclerostin's effects on metabolism and bone mass. A number of recent studies, including some from our own laboratory, indicate that Wnt signaling regulates the intermediary metabolism of the osteoblast and thereby influences metabolic homeostasis (43–46). The coexistence of a high bone mass phenotype because of increased Wnt signaling and increased fat mass in ObΔLrp4 mice indicates that the effect of sclerostin on adipose tissue mass and metabolism is distinct from its effect on bone metabolism.

In summary, this study elaborates the mechanisms by which sclerostin influences whole-body metabolism and the mechanisms of cross-talk between adipose tissue and bone. We expect that it will have important implications for the use of sclerostin-neutralizing therapeutic agents intended to treat osteopenia/osteoporosis but may also be useful in the treatment of obesity and metabolic disease.

Experimental procedures

Mouse models

The Institutional Animal Care and Use Committee of the Johns Hopkins University approved all procedures involving mice. $Lrp4^{flox/flox}$ mice, in which exon 1 of the *Lrp4* gene is flanked by loxP sites, were described previously (26, 32). To generate adipocyte- and osteoblast-specific mutants, mice were crossed with AdipoQ-Cre mice (34) and Ocn-Cre mice (47), respectively. The resulting $Lrp4^{flox/+}$; $Cre^{+/-}$ progeny were then backcrossed to $Lrp4^{flox/flox}$ mice to generate the tissue-specific knockouts. Breeding pairs of $Lrp4^{flox/flox}$; $Cre^{+/-}$ and $Lrp4^{flox/flox}$ mice were used to generated control ($Lrp4^{flox/flox}$ mice) and knockout littermates for all studies. $Sost^{-/-}$ mice ($Sost^{tm1(KOMP)Vlcg}$) were originally obtained from the KOMP repository and reconstituted as described previously (3). For genetic epistasis studies, $Lrp4^{flox/flox}$; AdipoQ-$Cre^{+/-}$ mice were cross-bred with $Sost^{+/-}$ mice to generate littermates with the four required genotypes: $Sost^{+/+}$; $Lrp4^{flox/+}$ (referred to as control), $Sost^{+/+}$; $Lrp4^{flox/+}$; AdipoQ-$Cre^{+/-}$ (referred to as AdΔLrp4/+), $Sost^{+/-}$; $Lrp4^{flox/+}$ (referred to as $Sost^{+/-}$), and $Sost^{+/}$; $Lrp4^{flox/+}$; AdipoQ-$Cre^{+/-}$ (referred to as AdΔLrp4/+; $Sost^{+/-}$).

All mice were maintained on a C57BL/6 background. Mice were housed on ventilated racks on a 14-h light/10-h dark cycle and fed *ad libitum* with a standard chow diet (Extruded Global Rodent Diet, Harlan Laboratories).

Culture of primary adipocytes

Primary adipocyte precursors were harvested from the inguinal fat pads by collagenase digestion as described previously (48) and cultured in DMEM (Gibco) containing 10% FBS (Sigma-Aldrich). Lrp4 gene deletion *in vitro* was induced by infection with an adenovirus directing the expression of Cre recombinase (multiplicity of infection 100, Vector Biolabs). An adenovirus directing the expression of GFP was used as a control. Upon reaching confluence, cells were induced to differentiate by treatment with 0.5 mM 3-isobutyl-1-methylxanthin, 1 μM dexamethasone, and 167 nM insulin for 2 days, followed by continued culture in 167 nM insulin, which was changed every 2 days thereafter until analysis. Recombinant mouse sclerostin (R&D Systems) and Bmp4 (PeproTech) were replaced with each medium change. Oil Red O staining was carried out according to a standard technique.

Fatty acid metabolism

Fatty acid oxidation by cultured adipocytes was measured in flasks with stoppers equipped with center wells as described previously (49). Reactions were incubated at 37 °C in medium containing 0.5 mM L-carnitine, 0.2% BSA, and [^{14}C]oleate (PerkinElmer Life Sciences). Expired $^{14}CO_2$ was captured and counted by addition of 1 N perchloric acid to the reaction mixture and 1 M NaOH to the center well containing Whatman filter paper. To measure *de novo* lipogenesis, cellular lipids were

collected by the Folch method 3 h after administration of 0.1 μCi [^{3}H]acetate.

Gene expression studies

Total RNA was extracted using TRIzol (Life Technologies). For adipose tissue, samples were centrifuged prior to RNA purification to remove excess lipid. Bone samples were washed free of marrow before RNA isolation. Reverse transcriptase reactions were carried out using 1 μg of RNA and the iScript cDNA synthesis system (Bio-Rad). Real-time qPCR was carried out using iQ Sybr Green Supermix (Bio-Rad) and primer sequences obtained from PrimerBank (http://pga.mgh.harvard.edu/primerbank/index.html).[4] Reactions were normalized to endogenous 18S reference transcripts. Antibodies for Western blotting were obtained from Cell Signal Technologies (phospho-Akt, catalog no. 4060; Akt, catalog no. 4685; phospho-Smad1/5/9, catalog no. 13820; and Smad1, catalog no. 9743) and Invitrogen (Lrp4, catalog no. PA5-68218; Lrp5, 36-5400; and Lrp6, catalog no. PA5-67902).

Metabolic phenotyping and bioassays

Whole-body fat and lean mass were assessed by qNMR (echo MRI). Plasma triglycerides and free fatty acids were measured colorimetrically (Sigma) in plasma collected 3 h after initiation of the light cycle. Serum sclerostin and insulin were measured in plasma by ELISA (Alpco). Glucose levels were measured using a Bayer Contour handheld glucose monitor. For glucose tolerance testing, glucose (2 g/kg of BW) was injected i.p. after a 6-h fast. For insulin tolerance testing, mice were fasted for 4 h and then injected i.p. with insulin (0.25 units/kg of BW). Insulin signaling in WAT was assessed by injection of insulin (1 units/kg of BW) into the portal vein before excising tissue and snap-freezing for immunoblot analysis. Tissue for histological analysis was collected at necropsy, weighed, and then fixed in 4% paraformaldehyde before embedding and sectioning. Adipocyte size was assessed using ImageJ. DNA was isolated from WAT using the Quick-DNA Universal Kit (Zymo Research) following proteinase K digestion. Ki67 (Abcam, ab15580) staining was performed on frozen adipose tissue sections according to standard immunohistochemical techniques.

Imaging

High-resolution images of the mouse femur were acquired using a desktop microtomographic imaging system (Skyscan 1275, Bruker) in accordance with the recommendations of the American Society for Bone and Mineral Research (50). Bones were scanned at 65 keV and 153 μA using a 1.0-mm aluminum filter with an isotropic voxel size of 10 μm. Trabecular bone parameters were assessed 500 μm proximal to the growth plate and extending for 2 mm (200 CT slices).

Statistical analysis

All results are expressed as mean ± S.E. Statistical analyses were performed using unpaired, two-tailed Student's t test or analysis of variance followed by post hoc tests. A p value of less than 0.05 was considered significant (*, $p \leq 0.05$ in all figures).

[4] Please note that the JBC is not responsible for the long-term archiving and maintenance of this site or any other third party–hosted site.

Author contributions—S. P. K., M. J. W., T. L. C., and R. C. R. conceptualization; S. P. K., H. D., Z. L., P. K., C. B., and R. C. R. data curation; S. P. K., M. J. W., and T. L. C. formal analysis; S. P. K., H. D., Z. L., P. K., C. B., and R. C. R. investigation; L. M. and W.-C. X. resources; M. J. W., T. L. C., and R. C. R. writing-review and editing; R. C. R. supervision; R. C. R. funding acquisition; R. C. R. writing-original draft; R. C. R. project administration.

Acknowledgments—We thank Nadine Forbes-McBean for assistance with qNMR analysis.

References

1. Kajimura, D., Lee, H. W., Riley, K. J., Arteaga-Solis, E., Ferron, M., Zhou, B., Clarke, C. J., Hannun, Y. A., DePinho, R. A., Guo, X. E., Guo, E. X., Mann, J. J., and Karsenty, G. (2013) Adiponectin regulates bone mass via opposite central and peripheral mechanisms through FoxO1. *Cell Metab.* **17,** 901–915 CrossRef Medline
2. Ducy, P., Amling, M., Takeda, S., Priemel, M., Schilling, A. F., Beil, F. T., Shen, J., Vinson, C., Rueger, J. M., and Karsenty, G. (2000) Leptin inhibits bone formation through a hypothalamic relay: a central control of bone mass. *Cell* **100,** 197–207 CrossRef Medline
3. Kim, S. P., Frey, J. L., Li, Z., Kushwaha, P., Zoch, M. L., Tomlinson, R. E., Da, H., Aja, S., Noh, H. L., Kim, J. K., Hussain, M. A., Thorek, D. L. J., Wolfgang, M. J., and Riddle, R. C. (2017) Sclerostin influences body composition by regulating catabolic and anabolic metabolism in adipocytes. *Proc. Natl. Acad. Sci. U.S.A.* **114,** E11238–E11247 CrossRef Medline
4. Lee, N. K., Sowa, H., Hinoi, E., Ferron, M., Ahn, J. D., Confavreux, C., Dacquin, R., Mee, P. J., McKee, M. D., Jung, D. Y., Zhang, Z., Kim, J. K., Mauvais-Jarvis, F., Ducy, P., and Karsenty, G. (2007) Endocrine regulation of energy metabolism by the skeleton. *Cell* **130,** 456–469 CrossRef Medline
5. Ferron, M., Hinoi, E., Karsenty, G., and Ducy, P. (2008) Osteocalcin differentially regulates β cell and adipocyte gene expression and affects the development of metabolic diseases in wild-type mice. *Proc. Natl. Acad. Sci. U.S.A.* **105,** 5266–5270 CrossRef Medline
6. Ge, C., Cawthorn, W. P., Li, Y., Zhao, G., Macdougald, O. A., and Franceschi, R. T. (2016) Reciprocal control of osteogenic and adipogenic differentiation by ERK/MAP kinase phosphorylation of Runx2 and PPARγ transcription factors. *J. Cell. Physiol.* **231,** 587–596 CrossRef Medline
7. Chen, D., Ji, X., Harris, M. A., Feng, J. Q., Karsenty, G., Celeste, A. J., Rosen, V., Mundy, G. R., and Harris, S. E. (1998) Differential roles for bone morphogenetic protein (BMP) receptor type IB and IA in differentiation and specification of mesenchymal precursor cells to osteoblast and adipocyte lineages. *J. Cell Biol.* **142,** 295–305 CrossRef Medline
8. Bennett, C. N., Ross, S. E., Longo, K. A., Bajnok, L., Hemati, N., Johnson, K. W., Harrison, S. D., and MacDougald, O. A. (2002) Regulation of Wnt signaling during adipogenesis. *J. Biol. Chem.* **277,** 30998–31004 CrossRef Medline
9. Kang, S., Bennett, C. N., Gerin, I., Rapp, L. A., Hankenson, K. D., and Macdougald, O. A. (2007) Wnt signaling stimulates osteoblastogenesis of mesenchymal precursors by suppressing CCAAT/enhancer-binding protein α and peroxisome proliferator-activated receptor γ. *J. Biol. Chem.* **282,** 14515–14524 CrossRef Medline
10. Li, X., Ominsky, M. S., Niu, Q. T., Sun, N., Daugherty, B., D'Agostin, D., Kurahara, C., Gao, Y., Cao, J., Gong, J., Asuncion, F., Barrero, M., Warmington, K., Dwyer, D., Stolina, M., *et al.* (2008) Targeted deletion of the sclerostin gene in mice results in increased bone formation and bone strength. *J. Bone Miner. Res.* **23,** 860–869 CrossRef Medline
11. van Bezooijen, R. L., Roelen, B. A., Visser, A., van der Wee-Pals, L., de Wilt, E., Karperien, M., Hamersma, H., Papapoulos, S. E., ten Dijke, P., and Löwik, C. W. (2004) Sclerostin is an osteocyte-expressed negative regulator of bone formation, but not a classical BMP antagonist. *J. Exp. Med.* **199,** 805–814 CrossRef Medline

12. Bourhis, E., Wang, W., Tam, C., Hwang, J., Zhang, Y., Spittler, D., Huang, O. W., Gong, Y., Estevez, A., Zilberleyb, I., Rouge, L., Chiu, C., Wu, Y., Costa, M., Hannoush, R. N., *et al.* (2011) Wnt antagonists bind through a short peptide to the first β-propeller domain of LRP5/6. *Structure* **19,** 1433–1442 CrossRef Medline
13. Gong, Y., Bourhis, E., Chiu, C., Stawicki, S., DeAlmeida, V. I., Liu, B. Y., Phamluong, K., Cao, T. C., Carano, R. A., Ernst, J. A., Solloway, M., Rubinfeld, B., Hannoush, R. N., Wu, Y., Polakis, P., and Costa, M. (2010) Wnt isoform-specific interactions with coreceptor specify inhibition or potentiation of signaling by LRP6 antibodies. *PLoS ONE* **5,** e12682 CrossRef Medline
14. Holdsworth, G., Slocombe, P., Doyle, C., Sweeney, B., Veverka, V., Le Riche, K., Franklin, R. J., Compson, J., Brookings, D., Turner, J., Kennedy, J., Garlish, R., Shi, J., Newnham, L., McMillan, D., *et al.* (2012) Characterization of the interaction of sclerostin with the low density lipoprotein receptor-related protein (LRP) family of Wnt co-receptors. *J. Biol. Chem.* **287,** 26464–26477 CrossRef Medline
15. Day, T. F., Guo, X., Garrett-Beal, L., and Yang, Y. (2005) Wnt/β-catenin signaling in mesenchymal progenitors controls osteoblast and chondrocyte differentiation during vertebrate skeletogenesis. *Dev. Cell* **8,** 739–750 CrossRef Medline
16. Holmen, S. L., Zylstra, C. R., Mukherjee, A., Sigler, R. E., Faugere, M. C., Bouxsein, M. L., Deng, L., Clemens, T. L., and Williams, B. O. (2005) Essential role of β-catenin in postnatal bone acquisition. *J. Biol. Chem.* **280,** 21162–21168 CrossRef Medline
17. García-Martín, A., Rozas-Moreno, P., Reyes-García, R., Morales-Santana, S., García-Fontana, B., García-Salcedo, J. A., and Muñoz-Torres, M. (2012) Circulating levels of sclerostin are increased in patients with type 2 diabetes mellitus. *J. Clin. Endocrinol. Metab.* **97,** 234–241 CrossRef Medline
18. Gaudio, A., Privitera, F., Battaglia, K., Torrisi, V., Sidoti, M. H., Pulvirenti, I., Canzonieri, E., Tringali, G., and Fiore, C. E. (2012) Sclerostin levels associated with inhibition of the Wnt/β-catenin signaling and reduced bone turnover in type 2 diabetes mellitus. *J. Clin. Endocrinol. Metab.* **97,** 3744–3750 CrossRef Medline
19. Gennari, L., Merlotti, D., Valenti, R., Ceccarelli, E., Ruvio, M., Pietrini, M. G., Capodarca, C., Franci, M. B., Campagna, M. S., Calabrò, A., Cataldo, D., Stolakis, K., Dotta, F., and Nuti, R. (2012) Circulating sclerostin levels and bone turnover in type 1 and type 2 diabetes. *J. Clin. Endocrinol. Metab.* **97,** 1737–1744 CrossRef Medline
20. Urano, T., Shiraki, M., Ouchi, Y., and Inoue, S. (2012) Association of circulating sclerostin levels with fat mass and metabolic disease-related markers in Japanese postmenopausal women. *J. Clin. Endocrinol. Metab.* **97,** E1473–E1477 CrossRef Medline
21. Amrein, K., Amrein, S., Drexler, C., Dimai, H. P., Dobnig, H., Pfeifer, K., Tomaschitz, A., Pieber, T. R., and Fahrleitner-Pammer, A. (2012) Sclerostin and its association with physical activity, age, gender, body composition, and bone mineral content in healthy adults. *J. Clin. Endocrinol. Metab.* **97,** 148–154 CrossRef Medline
22. Daniele, G., Winnier, D., Mari, A., Bruder, J., Fourcaudot, M., Pengou, Z., Tripathy, D., Jenkinson, C., and Folli, F. (2015) Sclerostin and insulin resistance in prediabetes: evidence of a cross talk between bone and glucose metabolism. *Diabetes Care* **38,** 1509–1517 CrossRef Medline
23. Wdrychowicz, A., Sztefko, K., and Starzyk, J. B. (2019) Sclerostin and its association with insulin resistance in children and adolescents. *Bone* **120,** 232–238 Medline
24. Yang, T., and Williams, B. O. (2017) Low-density lipoprotein receptor-related proteins in skeletal development and disease. *Physiol. Rev.* **97,** 1211–1228 CrossRef Medline
25. Weatherbee, S. D., Anderson, K. V., and Niswander, L. A. (2006) LDL-receptor-related protein 4 is crucial for formation of the neuromuscular junction. *Development* **133,** 4993–5000 CrossRef Medline
26. Wu, H., Lu, Y., Shen, C., Patel, N., Gan, L., Xiong, W. C., and Mei, L. (2012) Distinct roles of muscle and motoneuron LRP4 in neuromuscular junction formation. *Neuron* **75,** 94–107 CrossRef Medline
27. Leupin, O., Piters, E., Halleux, C., Hu, S., Kramer, I., Morvan, F., Bouwmeester, T., Schirle, M., Bueno-Lozano, M., Fuentes, F. J., Itin, P. H., Boudin, E., de Freitas, F., Jennes, K., Brannetti, B., *et al.* (2011) Bone overgrowth-associated mutations in the LRP4 gene impair sclerostin facilitator function. *J. Biol. Chem.* **286,** 19489–19500 CrossRef Medline
28. Balemans, W., Ebeling, M., Patel, N., Van Hul, E., Olson, P., Dioszegi, M., Lacza, C., Wuyts, W., Van Den Ende, J., Willems, P., Paes-Alves, A. F., Hill, S., Bueno, M., Ramos, F. J., Tacconi, P., *et al.* (2001) Increased bone density in sclerosteosis is due to the deficiency of a novel secreted protein (SOST). *Hum. Mol. Genet.* **10,** 537–543 CrossRef Medline
29. Loots, G. G., Kneissel, M., Keller, H., Baptist, M., Chang, J., Collette, N. M., Ovcharenko, D., Plajzer-Frick, I., and Rubin, E. M. (2005) Genomic deletion of a long-range bone enhancer misregulates sclerostin in Van Buchem disease. *Genome Res.* **15,** 928–935 CrossRef Medline
30. Staehling-Hampton, K., Proll, S., Paeper, B. W., Zhao, L., Charmley, P., Brown, A., Gardner, J. C., Galas, D., Schatzman, R. C., Beighton, P., Papapoulos, S., Hamersma, H., and Brunkow, M. E. (2002) A 52-kb deletion in the SOST-MEOX1 intergenic region on 17q12-q21 is associated with van Buchem disease in the Dutch population. *Am. J. Med. Genet* **110,** 144–152 CrossRef Medline
31. Chang, M. K., Kramer, I., Huber, T., Kinzel, B., Guth-Gundel, S., Leupin, O., and Kneissel, M. (2014) Disruption of Lrp4 function by genetic deletion or pharmacological blockade increases bone mass and serum sclerostin levels. *Proc. Natl. Acad. Sci. U.S.A.* **111,** E5187–E5195 CrossRef Medline
32. Xiong, L., Jung, J. U., Wu, H., Xia, W. F., Pan, J. X., Shen, C., Mei, L., and Xiong, W. C. (2015) Lrp4 in osteoblasts suppresses bone formation and promotes osteoclastogenesis and bone resorption. *Proc. Natl. Acad. Sci. U.S.A.* **112,** 3487–3492 CrossRef Medline
33. Jho, E. H., Zhang, T., Domon, C., Joo, C. K., Freund, J. N., and Costantini, F. (2002) Wnt/β-catenin/Tcf signaling induces the transcription of Axin2, a negative regulator of the signaling pathway. *Mol. Cell. Biol.* **22,** 1172–1183 CrossRef Medline
34. Eguchi, J., Wang, X., Yu, S., Kershaw, E. E., Chiu, P. C., Dushay, J., Estall, J. L., Klein, U., Maratos-Flier, E., and Rosen, E. D. (2011) Transcriptional control of adipose lipid handling by IRF4. *Cell Metab.* **13,** 249–259 CrossRef Medline
35. Modica, S., Straub, L. G., Balaz, M., Sun, W., Varga, L., Stefanicka, P., Profant, M., Simon, E., Neubauer, H., Ukropcova, B., Ukropec, J., and Wolfrum, C. (2016) Bmp4 promotes a brown to white-like adipocyte shift. *Cell Rep.* **16,** 2243–2258 CrossRef Medline
36. Christodoulides, C., Laudes, M., Cawthorn, W. P., Schinner, S., Soos, M., O'Rahilly, S., Sethi, J. K., and Vidal-Puig, A. (2006) The Wnt antagonist Dickkopf-1 and its receptors are coordinately regulated during early human adipogenesis. *J. Cell Sci.* **119,** 2613–2620 CrossRef Medline
37. Longo, K. A., Wright, W. S., Kang, S., Gerin, I., Chiang, S. H., Lucas, P. C., Opp, M. R., and MacDougald, O. A. (2004) Wnt10b inhibits development of white and brown adipose tissues. *J. Biol. Chem.* **279,** 35503–35509 CrossRef Medline
38. Semënov, M., Tamai, K., and He, X. (2005) SOST is a ligand for LRP5/LRP6 and a Wnt signaling inhibitor. *J. Biol. Chem.* **280,** 26770–26775 CrossRef Medline
39. Choi, H. Y., Dieckmann, M., Herz, J., and Niemeier, A. (2009) Lrp4, a novel receptor for Dickkopf 1 and sclerostin, is expressed by osteoblasts and regulates bone growth and turnover *in vivo*. *PLoS ONE* **4,** e7930 CrossRef Medline
40. Tang, W., Zeve, D., Suh, J. M., Bosnakovski, D., Kyba, M., Hammer, R. E., Tallquist, M. D., and Graff, J. M. (2008) White fat progenitor cells reside in the adipose vasculature. *Science* **322,** 583–586 CrossRef Medline
41. Jeffery, E., Berry, R., Church, C. D., Yu, S., Shook, B. A., Horsley, V., Rosen, E. D., and Rodeheffer, M. S. (2014) Characterization of Cre recombinase models for the study of adipose tissue. *Adipocyte* **3,** 206–211 CrossRef Medline
42. Brun, J., Berthou, F., Trajkovski, M., Maechler, P., Foti, M., and Bonnet, N. (2017) Bone regulates browning and energy metabolism through mature osteoblast/osteocyte PPARγ expression. *Diabetes* **66,** 2541–2554 CrossRef Medline
43. Karner, C. M., Esen, E., Okunade, A. L., Patterson, B. W., and Long, F. (2015) Increased glutamine catabolism mediates bone anabolism in response to WNT signaling. *J. Clin. Invest.* **125,** 551–562 CrossRef Medline

44. Esen, E., Chen, J., Karner, C. M., Okunade, A. L., Patterson, B. W., and Long, F. (2013) WNT-LRP5 signaling induces Warburg effect through mTORC2 activation during osteoblast differentiation. *Cell Metab.* **17,** 745–755 CrossRef Medline
45. Frey, J. L., Kim, S. P., Li, Z., Wolfgang, M. J., and Riddle, R. C. (2018) β-Catenin directs long-chain fatty acid catabolism in the osteoblasts of male mice. *Endocrinology* **159,** 272–284 CrossRef Medline
46. Frey, J. L., Li, Z., Ellis, J. M., Zhang, Q., Farber, C. R., Aja, S., Wolfgang, M. J., Clemens, T. L., and Riddle, R. C. (2015) Wnt-Lrp5 signaling regulates fatty acid metabolism in the osteoblast. *Mol. Cell. Biol.* **35,** 1979–1991 CrossRef Medline
47. Zhang, M., Xuan, S., Bouxsein, M. L., von Stechow, D., Akeno, N., Faugere, M. C., Malluche, H., Zhao, G., Rosen, C. J., Efstratiadis, A., and Clemens, T. L. (2002) Osteoblast-specific knockout of the insulin-like growth factor (IGF) receptor gene reveals an essential role of IGF signaling in bone matrix mineralization. *J. Biol. Chem.* **277,** 44005–44012 CrossRef Medline
48. Kir, S., White, J. P., Kleiner, S., Kazak, L., Cohen, P., Baracos, V. E., and Spiegelman, B. M. (2014) Tumour-derived PTH-related protein triggers adipose tissue browning and cancer cachexia. *Nature* **513,** 100–104 CrossRef Medline
49. Lee, J., Ellis, J. M., and Wolfgang, M. J. (2015) Adipose fatty acid oxidation is required for thermogenesis and potentiates oxidative stress-induced inflammation. *Cell Rep.* **10,** 266–279 CrossRef Medline
50. Bouxsein, M. L., Boyd, S. K., Christiansen, B. A., Guldberg, R. E., Jepsen, K. J., and Müller, R. (2010) Guidelines for assessment of bone microstructure in rodents using micro-computed tomography. *J. Bone Miner. Res.* **25,** 1468–1486 CrossRef Medline